Fuel 280 (2020) 118446

Contents lists available at ScienceDirect

Fuel

journal homepage: www.elsevier.com/locate/fuel

Full Length Article

Unveiling the critical role of p-d hybridization interaction in $M_{13-n}Ga_n$ clusters on CO_2 adsorption

Qingli Tang[a,b], Feng Shi[a], Kan Li[a], Wenchao Ji[c], Jerzy Leszczynski[d], Armistead G. Russell[e], Eric G. Eddings[f], Zhemin Shen[a,*], Maohong Fan[b,e,*]

[a] School of Environmental Science and Engineering, Shanghai Jiao Tong University, Shanghai 200240, PR China
[b] Departments of Chemical and Petroleum Engineering, University of Wyoming, Laramie 82071, WY, United States
[c] College of Resource and Environment, Anhui Science and Technology University, Fengyang 233100, Anhui, PR China
[d] Department of Chemistry, Physics and Atmospheric Sciences, Jackson State University, Jackson 39217, MS, United States
[e] School of Civil and Environmental Engineering, Georgia Institute of Technology, Atlanta 30332, GR, United States
[f] Department of Chemical Engineering, The University of Utah, Salt Lake City, UT 84112, United States

GRAPHICAL ABSTRACT

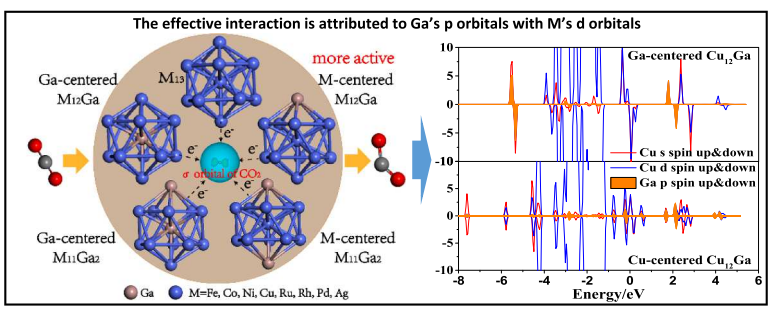

ARTICLE INFO

Keywords:
CO_2 adsorption
13-Atom clusters
Effects of Ga
Electronic properties

ABSTRACT

Inspired by conclusions of previous studies that Ga has the promoting effect on CO_2 conversion, we performed density functional theory (DFT) investigations of CO_2 adsorption on forty icosahedral (I_h) symmetry 13-atom clusters. They include M_{13}, Ga-centered $M_{12}Ga$, M-centered $M_{12}Ga$, Ga-centered $M_{11}Ga_2$ and M-centered $M_{11}Ga_2$ clusters (M = Fe, Co, Ni, Cu, Ru, Rh, Pd and Ag). Initially, the stabilities of these clusters were studied. The results show that Ga doped Cu, Pd, and Ag clusters are more stable than their pure metal analogues, and except Pd and Ag clusters, M-centered species are more stable than Ga-centered clusters. In addition, the activation of CO_2 on these clusters was studied. The results show that most of M-centered $M_{12}Ga$ clusters transfer more electron density to CO_2 than other corresponding Ga-doped analogues. The amount of Bader charge transfers has noteworthy linear relationship with the structural parameters of CO_2. DOS analyses show that empty σ orbital of CO_2 is acceptor of electrons from cluster. It is worth to mention that $Ag_{13-n}Ga_n$ clusters have little interaction with CO_2. To explain the effects of Ga on the adsorption of CO_2, the electronic properties of clusters were studied. The projected density of states (PDOSs), charge density differences, Bader charge transfers and electron localization functions (ELFs) analyses show that Ga transfers electron density to M atom, and the effective

* Corresponding authors at: 800 Dongchuan Road, Minhang District, Shanghai, 200240, China (Z. Shen). 1000 E University Ave., Laramie, WY 82071, United States (M. Fan).

E-mail addresses: zmshen@sjtu.edu.cn (Z. Shen), mfan@uwyo.edu (M. Fan).

https://doi.org/10.1016/j.fuel.2020.118446
Received 3 April 2020; Received in revised form 20 May 2020; Accepted 15 June 2020

interaction is attributed to the p orbitals of Ga with the d orbitals of M near Fermi level(0), mainly responsible for the activation of CO_2.

1. Introduction

It has been demonstrated that sub-nanometre sized metal clusters consisting of limited number of atoms with unique physical and chemical properties [1] have improved catalytic performances [2–5]. Experiments also showed that the sizes of metal catalysts can be tuned by the loading contents [3,6], which means that compared with bulk catalysts, clusters with a few atoms can largely reduce the loading amounts and thus reduce the costs of industrial processes. In addition, the electronic and magnetic properties of sub-nanometre sized clusters are largely changed compared to their bulk analogues and larger nanoparticles [1]. Among sub-nanometre sized clusters, transition metal 13-atom clusters TM_{13} (TM = Fe [7,8], Co [8], Ni [8,9], Cu [10,11], Pd [12], Ag [13], Pt [9,14–16] and Au [17]) have been extensively investigated experimentally and theoretically because of their large surface areas. In particular, TM_{13} clusters can exhibit a high symmetric I_h structure even though some do not represent the lowest energy structures, including Au_{13}[18], Pd_{13}[19], and Pt_{13}[20].

It is well known that CO_2 capture [21,22] and chemical and electrochemical processes for CO_2 reduction to fuels [23–27] have brought widespread attention of researchers because of its continuous increasing concentration in the atmosphere. Among the reduction products, methanol (CH_3OH) is an easily marketable and useful feedstock. Although the studies on effective catalysts aiming for CO_2 reduction to CH_3OH have emerged in numerous publications [28–32]; however, the existing catalysts still have a long way before commercial utilization due to the low process and cost-efficiency. Therefore, great efforts still have to be dedicated to the design of new catalysts.

A large number of experimental and theoretical studies proved that compared with monometallic catalysts, bimetallic catalysts have higher catalytic activities [12,33]. For all the bimetallic combinations applicable for CO_2 reduction to CH_3OH, Ga contained transition metal catalysts would be promising choices due to their good catalytic effects. For example, the studies performed by Studt et al. [34] and Fiordaliso et al. [35] respectively showed that Ni-Ga and Pd-Ga bimetallic catalysts are more effective for CO_2 reduction to methanol than traditional $Cu/ZnO/Al_2O_3$ catalysts. Ga plays an important role in the reaction. In Ga doped $Cu/ZnO/ZrO_2$ catalysts [36], the presence of Ga increases surface Cu and metallic Cu^0 and thus the active sites for CO_2 hydrogenation to CH_3OH due to the segregation of Cu to the surface. The same conclusion was obtained by Toyir et al. [37]. In addition, Collins et al. [38,39] concluded that on a Pd/Ga_2O_3 catalyst, CO_2 is stepwise hydrogenated to CH_3OH on the surface sites of gallium oxide in the process of CO_2 hydrogenation. In this reaction the role of Pd or Pd-Ga particles is to provide atomic hydrogen to the sites via spillover. Medina et al. [40] carried out a comparative study of Cu/SiO_2 and Ga doped Cu/SiO_2 in the hydrogenation of CO_2 to CH_3OH, and found that formate can adsorb on both Cu and Ga. This suggests that Ga may create new active sites for CH_3OH formation and thus cause the increase of CH_3OH formation rate.

With the development of computational approaches including DFT methods, more and more catalytic reactions could be investigated without spending much time and money. For example, theoretical study by Santiago-Rodríguez et al. [41] suggested that Ga doped Cu(1 1 1) surface may be among the promising catalysts for CO_2 hydrogenation. In particular, using computational methods the structure parameters and the electronic properties can be well described, providing basis for predicting their catalytic effects. Previous studies [8,42] showed that the activation of CO_2 is one of the most important descriptors in the CO_2 reduction process.

In this work, aiming to screening potential catalysts for CO_2 conversion, we designed a series of Ga doped I_h symmetry 13-atom clusters (M_{13}, Ga-centered $M_{12}Ga$, M-centered $M_{12}Ga$, Ga-centered $M_{11}Ga_2$ and M-centered $M_{11}Ga_2$ clusters (M = Fe, Co, Ni, Cu, Ru, Rh, Pd and Ag)) for the activation of CO_2 by using DFT level computational studies. The stabilities of these clusters were initially investigated; and then the adsorption activities of CO_2 were calculated. To further probe into the effect of Ga atoms on CO_2 adsorption, the electronic properties of $M_{13-n}Ga_n$ clusters were analyzed. The study can make advancement in understanding the effect of Ga in bimetallic catalysts towards the adsorption of CO_2, and provide the possibility of designing highly efficient catalysts for CO_2 conversion to CH_3OH.

2. Computational details

2.1. Computational methods

In this work, all the first principles calculations were performed by the Vienna ab initio simulation package (VASP) [43–45] code. The exchange-correlation function was described by the generalized gradient approximation (GGA) with the formula of Perdew-Burke-Ernzerhof (PBE)[46]. The projector augmented wave (PAW) [47,48] pseudopotentials was used to treat the ion-electron interactions. A plane wave cut off energy of 400 eV was used to expand the electron function. The Brillouin zone was only sampled on gamma point for the

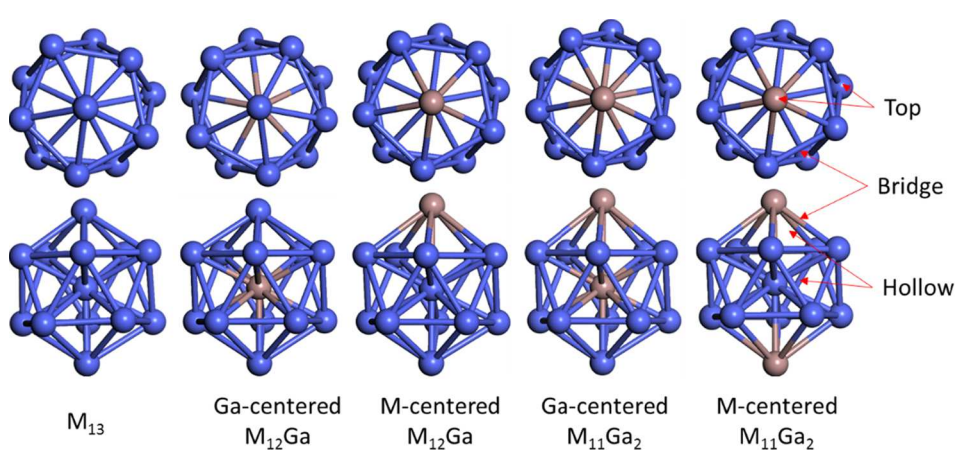

Fig. 1. The models of $M_{13-n}Ga_n$ clusters.

geometry optimizations. The criterions that were used to terminate the electronic and ionic calculation steps are 1.0×10^{-5} eV and 0.01 eV/Å, respectively.

2.2. Calculation models

Clusters' compositions and structures are important factors that affect their properties. The M_{13} clusters were initially built with highly symmetric I_h structures and $M_{12}Ga$ or $M_{11}Ga_2$ clusters were built based on optimized M_{13} clusters. In all simulations, the $M_{13-n}Ga_n$ (n = 0, 1, and 2) cluster was placed in a $20 \times 20 \times 20$ Å^3 cubic cell with periodic boundary conditions. The clusters' structures are shown in Fig. 1, and the average bond lengths are listed in Table S1 of Supplementary Materials. The adsorption activities of CO_2 were probed using the optimized structures of $M_{13-n}Ga_n$ clusters.

3. Results and discussions

3.1. Structure stabilities of $M_{13-n}Ga_n$ clusters

To evaluate the stabilities of $M_{13-n}Ga_n$ clusters, the binding energy per atom (E_b) is calculated, the used equation is as follows:

$$E_b = \frac{E_{M_{13-n}Ga_n} - (13-n)E_M - nE_{Ga}}{13} \quad (1)$$

where $E_{M_{13-n}Ga_n}$ is the total energy of $M_{13-n}Ga_n$ cluster; E_M and E_{Ga} represent the chemical potentials of M and Ga atoms, respectively. The lower the E_b is, the more stable the cluster is. The E_b of $M_{13-n}Ga_n$ clusters are listed in Table 1. As is shown for Fe, Co, Ni, Ru and Rh, the pure metal clusters have lower E_b than their corresponding Ga doped analogues, while for Cu, Pd, and Ag, Ga doped clusters have lower E_b than their pure metal compounds. The results suggest that Ga doped Cu, Pd, and Ag clusters are more stable than their pure analogues. For $M_{12}Ga$ clusters, M-centered $M_{12}Ga$ clusters have lower binding energies than the corresponding Ga-centered $M_{12}Ga$ clusters except $Pd_{12}Ga$. This suggests that M-centered structures are more stable than Ga-centered structures, except $Pd_{12}Ga$. For $M_{11}Ga_2$ clusters, except $Pd_{11}Ga_2$ and $Ag_{11}Ga_2$ clusters, the same conclusion as for the $M_{12}Ga$ species could be derived.

Additionally, to further evaluate the site preference of Ga atom in $M_{12}Ga$ and $M_{11}Ga_2$ clusters, its segregation energy (E_{seg}^{Ga}) is calculated, which is defined as

$$E_{seg}^{Ga} = E_{Ga-centered} - E_{M-centered} \quad (2)$$

where $E_{Ga-centered}$ and $E_{M-centered}$ represent the total energy of Ga-centered and M-centered $M_{12}Ga$ ($M_{11}Ga_2$) clusters, respectively. The negative value of E_{seg}^{Ga} demonstrates that Ga favors the central position, and positive value means that Ga tends towards the surface position. Table 2 lists the segregation energies of Ga in $M_{12}Ga$ and $M_{11}Ga_2$ clusters. It can be seen that except in $Pd_{12}Ga$ and $Ru_{12}Ga$, Ga prefers the surface position in all the other $M_{12}Ga$ clusters. It is worth to mention that for $Ru_{12}Ga$, surface Ga and center Ga atoms are compatible. Among $M_{11}Ga_2$ clusters, Ga also favors the surface position except in $Pd_{11}Ga_2$ and $Ag_{11}Ga_2$ clusters. The result is consistent with that obtained from evaluation of E_b.

Table 2
The segregation energy of Ga in $M_{12}Ga$ and $M_{11}Ga_2$ clusters.

clusters	E_{seg}^{Ga}/eV	clusters	E_{seg}^{Ga}/eV
$Fe_{12}Ga$	1.60	$Fe_{11}Ga_2$	1.28
$Co_{12}Ga$	2.35	$Co_{11}Ga_2$	2.03
$Ni_{12}Ga$	1.25	$Ni_{11}Ga_2$	1.95
$Cu_{12}Ga$	1.66	$Cu_{11}Ga_2$	0.75
$Ru_{12}Ga$	2.31	$Ru_{11}Ga_2$	2.00
$Rh_{12}Ga$	0.005	$Rh_{11}Ga_2$	0.79
$Pd_{12}Ga$	−0.81	$Pd_{11}Ga_2$	−0.49
$Ag_{12}Ga$	0.97	$Ag_{11}Ga_2$	−0.43

3.2. The adsorption characteristics of CO_2 on $M_{13-n}Ga_n$ clusters

3.2.1. Charge transfers between CO_2 and $M_{13-n}Ga_n$ cluster

Previous studies showed that charge transfers between substrate and CO_2 is a key descriptor that assesses the activation of CO_2 [8,49]. Bader charge is often useful for charge analysis [50–52]. Therefore, the adsorption of CO_2 on $M_{13-n}Ga_n$ clusters is checked on all potential sites (top, bridge, and hollow sites in Fig. 1). The Bader charge transfer of CO_2 is defined as follows,

$$T_{Bader-CO_2} = \sum VC_{atom-in-molecule} - \sum VC_{single-atom} \quad (3)$$

where $T_{Bader-CO_2}$ is the Bader charge transfer of CO_2, $\sum VC_{atom-in-molecule}$ is the sum of valence charge of each atom in CO_2 after adsorption, $\sum VC_{single-atom}$ is the sum of valence charge of each single atom in CO_2. The positive value of $T_{Bader-CO_2}$ represents CO_2 accepts electrons from clusters.

The structure with the highest Bader charge transfers (Table 3) from cluster to CO_2 is selected as the aim of this study for each $M_{13-n}Ga_n$ cluster. From Table 3, it can be seen that almost all the Ga doped clusters are characterized by higher Bader charge transfers than their corresponding pure metal clusters, except Ag. Among Ga doped clusters, M-centered $M_{12}Ga$ clusters have the highest values of the Bader charge transfers and the average charge transfers is 0.18 e higher than that of pure metal clusters. The adsorption structures of CO_2 on $M_{13-n}Ga_n$ clusters with the highest Bader charge transfer values are shown in Fig. S1 of Supplementary Materials. For all clusters, CO_2 prefers to adsorb on the M composed bridge or hollow sites.

To clearly understand the direction of the charge transfers, the charge density differences of CO_2 adsorbed on $Cu_{13-n}Ga_n$ clusters are calculated and shown in Fig. 2. The isosurfaces indicate that the charge density changes mainly occur near the adsorption sites, and the charge densities between C(O) and clusters increase and those between C and O decrease. It suggests that upon the bonding the bond strengths between substrate and CO_2 are enhanced, and the C-O bonds are weakened. This indicates that CO_2 is activated by $Cu_{13-n}Ga_n$ clusters.

Table 1
The binding energy per atom (E_b) of $M_{13-n}Ga_n$ clusters.

	E_b(eV/atom)		E_b(eV/atom)			E_b(eV/atom)	
			Ga-centered	M-centered		Ga-centered	M-centered
Fe_{13}	−3.49	$Fe_{12}Ga$	−3.31	−3.44	$Fe_{11}Ga_2$	−3.24	−3.34
Co_{13}	−3.31	$Co_{12}Ga$	−3.12	−3.30	$Co_{11}Ga_2$	−3.08	−3.23
Ni_{13}	−3.54	$Ni_{12}Ga$	−3.39	−3.49	$Ni_{11}Ga_2$	−3.32	−3.47
Cu_{13}	−2.25	$Cu_{12}Ga$	−2.17	−2.30	$Cu_{11}Ga_2$	−2.27	−2.32
Ru_{13}	−4.21	$Ru_{12}Ga$	−3.93	−4.11	$Ru_{11}Ga_2$	−3.83	−3.98
Rh_{13}	−3.98	$Rh_{12}Ga$	−3.93	−3.93	$Rh_{11}Ga_2$	−3.84	−3.90
Pd_{13}	−2.33	$Pd_{12}Ga$	−2.53	−2.47	$Pd_{11}Ga_2$	−2.63	−2.60
Ag_{13}	−1.57	$Ag_{12}Ga$	−1.59	−1.67	$Ag_{11}Ga_2$	−1.72	−1.68

Table 3
The highest Bader charge transfers of CO_2 for each $M_{13-n}Ga_n$ cluster.

	Bader (e)		Bader (e)			Bader (e)	
			Ga-centered	M-centered		Ga-centered	M-centered
Fe_{13}	0.77	$Fe_{12}Ga$	0.85	0.93	$Fe_{11}Ga_2$	0.81	0.90
Co_{13}	0.76	$Co_{12}Ga$	0.75	0.97	$Co_{11}Ga_2$	0.87	0.73
Ni_{13}	0.59	$Ni_{12}Ga$	0.64	0.80	$Ni_{11}Ga_2$	0.77	0.52
Cu_{13}	0.53	$Cu_{12}Ga$	0.50	0.72	$Cu_{11}Ga_2$	0.61	0.56
Ru_{13}	0.89	$Ru_{12}Ga$	0.90	1.14	$Ru_{11}Ga_2$	1.02	1.04
Rh_{13}	0.65	$Rh_{12}Ga$	0.76	0.74	$Rh_{11}Ga_2$	0.80	0.88
Pd_{13}	0.43	$Pd_{12}Ga$	0.57	0.59	$Pd_{11}Ga_2$	0.64	0.50
Ag_{13}	0.10	$Ag_{12}Ga$	0.11	0.08	$Ag_{11}Ga_2$	0.09	0.08

3.2.2. Structural parameters of adsorbed CO_2

Most of studies showed that the adsorption geometry of CO_2 on metal surfaces [53] or clusters [8] is in a "V" shape. The structure parameters, including angles and the average bond lengths of adsorbed CO_2 are listed in Table S2 of Supplementary Materials. The correlations between Bader charge transfers and the angles and the average bond lengths of CO_2 are calculated for all the considered $M_{13-n}Ga_n$ clusters. As shown in Fig. 3, the Pearson correlation coefficients are as high as 0.89, and 0.94 for angles and average bond lengths of CO_2, respectively. It suggests that there are obvious linear relationships between Bader charge transfers and the structural parameters of CO_2. In other words, the activation of CO_2 can be reflected on the degree of its structure deformation.

3.2.3. Adsorption energies of CO_2

The adsorption energy (E_{ads}) of adsorbate is often used to measure the interaction between adsorbate and substrate. In this study, the E_{ads} of CO_2 on $M_{13-n}Ga_n$ cluster is defined as

$$E_{ads} = E_{total} - E_{M_{13-n}Ga_n} - E_{CO_2} \quad (4)$$

where E_{total} is the total energy of adsorbed CO_2 on $M_{13-n}Ga_n$ cluster, $E_{M_{13-n}Ga_n}$ is the energy of bare $M_{13-n}Ga_n$ cluster, and E_{CO_2} represents the energy of CO_2 in gas phase. The E_{ads} of CO_2 are listed in Table S2 of Supplementary Materials.

Similarly, the correlation of Bader charge transfers and E_{ads} is calculated (Fig. 4). The Pearson correlation coefficient is 0.78, which indicates that the Bader charge transfers have lower correlation with E_{ads} than with the angles and the average bond lengths of CO_2. Therefore, compared with structural parameters, E_{ads} may not be a good descriptor to reflect the degree of CO_2 activation.

3.2.4. DOS analysis of CO_2 adsorption

To obtain better insight into the nature of CO_2 adsorption on $M_{13-n}Ga_n$ clusters, the DOS of some clusters and CO_2 before and after interaction are calculated and shown in Fig. 5. In Fig. 5(a)–(e), (1) represents the DOS projected on clusters' s and d orbitals before CO_2 adsorption; (4) is the DOS of CO_2 before adsorption; (2) and (3) are the DOS projected on cluster's s and d orbitals and the DOS projected on CO_2 after CO_2 adsorption, respectively. Fig. 5(a) displays the DOS of CO_2 and Ag_{13} before and after adsorption. It can be seen that during interaction of CO_2 and Ag_{13} clusters, the empty σ orbital of CO_2 and the s and d orbitals of Ag_{13} clusters change only slightly. It means that there is no electron transfer between Ag_{13} and CO_2. Whereas, for the adsorption of CO_2 on Ni_{13} and Cu_{13} clusters (Fig. 5(b) and (c)), the empty orbital of CO_2 changes significantly, and it has a little overlap with the cluster's s and d orbitals below the Fermi-level(0). This suggests that CO_2 obtained electrons from Ni_{13} or Cu_{13} clusters and formed $CO_2^{\delta-}$. Usually, the orbitals below Fermi level(0) are electron occupied orbitals; on the contrary, the orbitals above Fermi level(0) are electron unoccupied orbitals. In addition, the antibonding of s and d orbitals of clusters are above the Fermi level(0), which benefits the adsorption. The results obtained from Bader charge transfers also well support these conclusions. Comparing Fig. 5(c)–(e), one can see that the σ orbital of CO_2 drops lower on Cu-centered $Cu_{12}Ga$ cluster compared to Cu_{13} and Ga-centered $Cu_{12}Ga$ clusters. It means that on Cu-centered $Cu_{12}Ga$ cluster the adsorption of CO_2 is stronger. The results are consistent with that conclusions obtained from Bader charge transfer values.

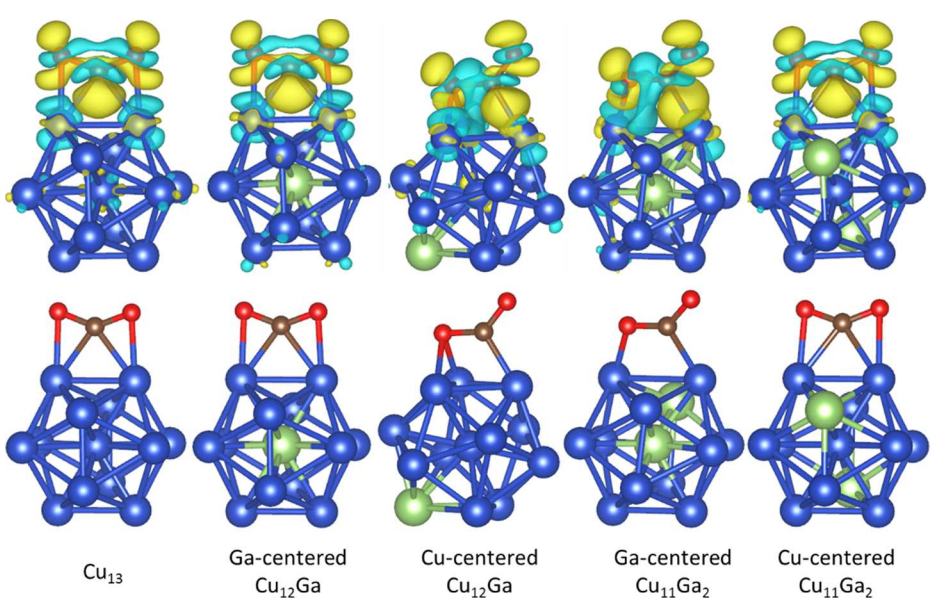

Fig. 2. Charge density differences of CO_2 on $Cu_{13-n}Ga_n$ clusters. Blue, green, brown and red balls are Cu, Ga, C and O atoms, respectively. Cyan and yellow represent the charge depletion and accumulation, respectively. (For interpretation of the references to colour in this figure legend, the reader is referred to the web version of this article.)

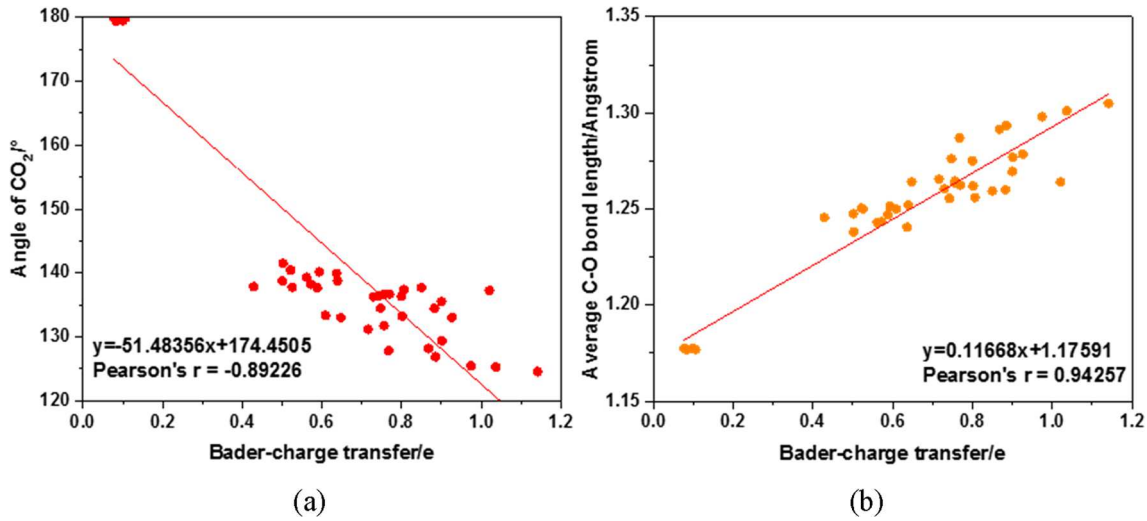

Fig. 3. The correlation between (a) Bader charge transfers from clusters to CO_2 and angles of adsorbed CO_2, and (b) Bader charge transfers from clusters to CO_2 and average C-O bond lengths of adsorbed CO_2.

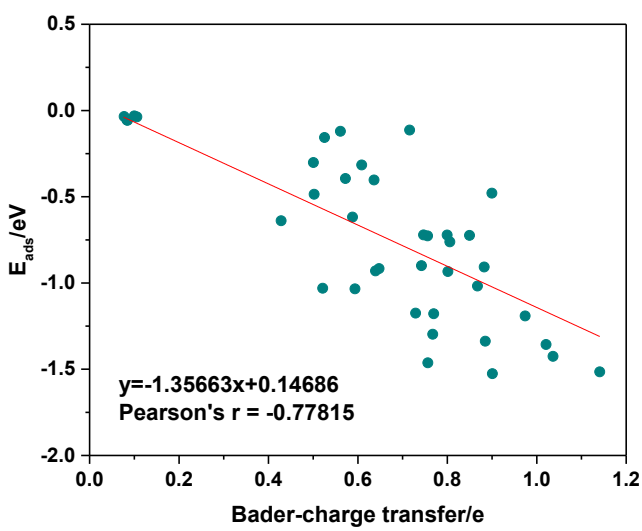

Fig. 4. The correlation between Bader charge transfers from clusters to CO_2 and E_{ads}.

3.3. The effects of doped Ga on CO_2 adsorption

3.3.1. The d-band center of $M_{13-n}Ga_n$ clusters and the influence on CO_2 adsorption

The d-band centers of $M_{13-n}Ga_n$ clusters are shown in Fig. 6(a). For 3d M_{13} clusters, the d-band center shift-up from Fe to Ni, while Cu has the lowest d-band center. However, for Ga replaced 3d M_{13} clusters, the $Co_{12}Ga$ and $Co_{11}Ga_2$ have lower d-band center than $Fe_{12}Ga$ and $Fe_{11}Ga_2$ clusters, respectively. For 4d M_{13} clusters, the d-band centers follow the same order: $Ag_{13-n}Ga_n$ < $Ru_{13-n}Ga_n$ < $Rh_{13-n}Ga_n$ < $Pd_{13-n}Ga_n$. $Ag_{13-n}Ga_n$ clusters have the lowest d-bands centers among all the corresponding clusters, then are $Cu_{13-n}Ga_n$ clusters. In general, compared with the d-band centers of pure metal clusters, their corresponding Ga doped clusters' d-band centers shift-up.

The correlation between Bader charge transfer values from clusters to CO_2 and d-band centers of clusters is calculated for M_{13}, Ga-centered $M_{12}Ga$, M-centered $M_{12}Ga$, Ga-centered $M_{11}Ga_2$, and M-centered $M_{11}Ga_2$ clusters (Fig. 6(b)). The results show that Bader charge transfers between substrate and CO_2 have notable linear relationship with d-band centers of substrates for each type of clusters with all Pearson correlation coefficients higher than 0.74. The results are consistent with previous studies that the higher the d-band center is, the more active the catalyst is [54–56]. Therefore, the doping by Ga makes the 13 atom metal clusters more active.

3.3.2. Electronic properties of Ga doped $M_{13-n}Ga_n$ clusters and the influence on CO_2 adsorption

To find out the nature of the Ga doped M_{13} clusters, the Bader charge transfer of Ga and the charge density differences are calculated (Table S3 and Fig. S2 in Supplementary Materials, respectively). The Bader charge transfer of Ga is defined as

$$T_{Bader-Ga} = \sum VC_{Ga-in-molecule} - \sum VC_{Ga} \tag{5}$$

where $T_{Bader-Ga}$ is the Bader charge transfer of Ga, $\sum VC_{Ga-in-molecule}$ is the sum of valence charge of Ga in $M_{13-n}Ga_n$ cluster, $\sum VC_{Ga}$ is the sum of valence charge of Ga atoms. The negative value of $T_{Bader-Ga}$ represents Ga has lost electrons.

By taking the example of Ga doped $Cu_{13-n}Ga_n$ clusters, the Bader charge transfer values from Ga to Cu amount to 0.69 and 0.26 e in Ga-centered and Cu-centered $Cu_{12}Ga$ clusters, respectively. In Ga-centered and Cu-centered $Cu_{11}Ga_2$ clusters, those values are 1.07 and 0.97 e. Besides these, there are also charge transfers among Cu atoms. The charge density differences of $Cu_{13-n}Ga_n$ clusters are shown in Fig. 7. It can be seen that electron density only accumulates between Cu atoms, and Ga atom transfers electrons to Cu atoms. Although Ga atom does transfer electrons to M in Ga doped $M_{13-n}Ga_n$ clusters, the number of electron transfers from Ga to M has no relation with the degree of CO_2 activation mentioned above. It is worth to note that CO_2 is far away from Ga atom after optimizing all the configurations, in which CO_2 is initially located at the top of Ga. This can be explained by the charge density difference of $M_{13-n}Ga_n$ clusters that indicates little electron accumulation around Ga atom, and thus there is no electron transfer from Ga to CO_2.

The ELF is a useful descriptor that is based on orbital wavefunctions used to classify chemical bonds [57,58]. Its value range is defined in [0,1]. The closer to 1 the ELF value is, the more localized the electron is. It means there is covalent bond, lone pair or atomic inner shell. While ELF = 0 represents that there are no electrons. When the value is around 0.5, it means there is metal free electron gas. To gain further insight into the bond classification, the ELFs related to the plane along the central line of $M_{13-n}Ga_n$ clusters are calculated, which are shown in Fig. S3 of Supplementary Materials. Take the ELFs of $Cu_{13-n}Ga_n$ clusters for example (Fig. 8), it can be seen that for surface Ga, there are localized electrons (lone pair in s orbital) at the center position of Ga

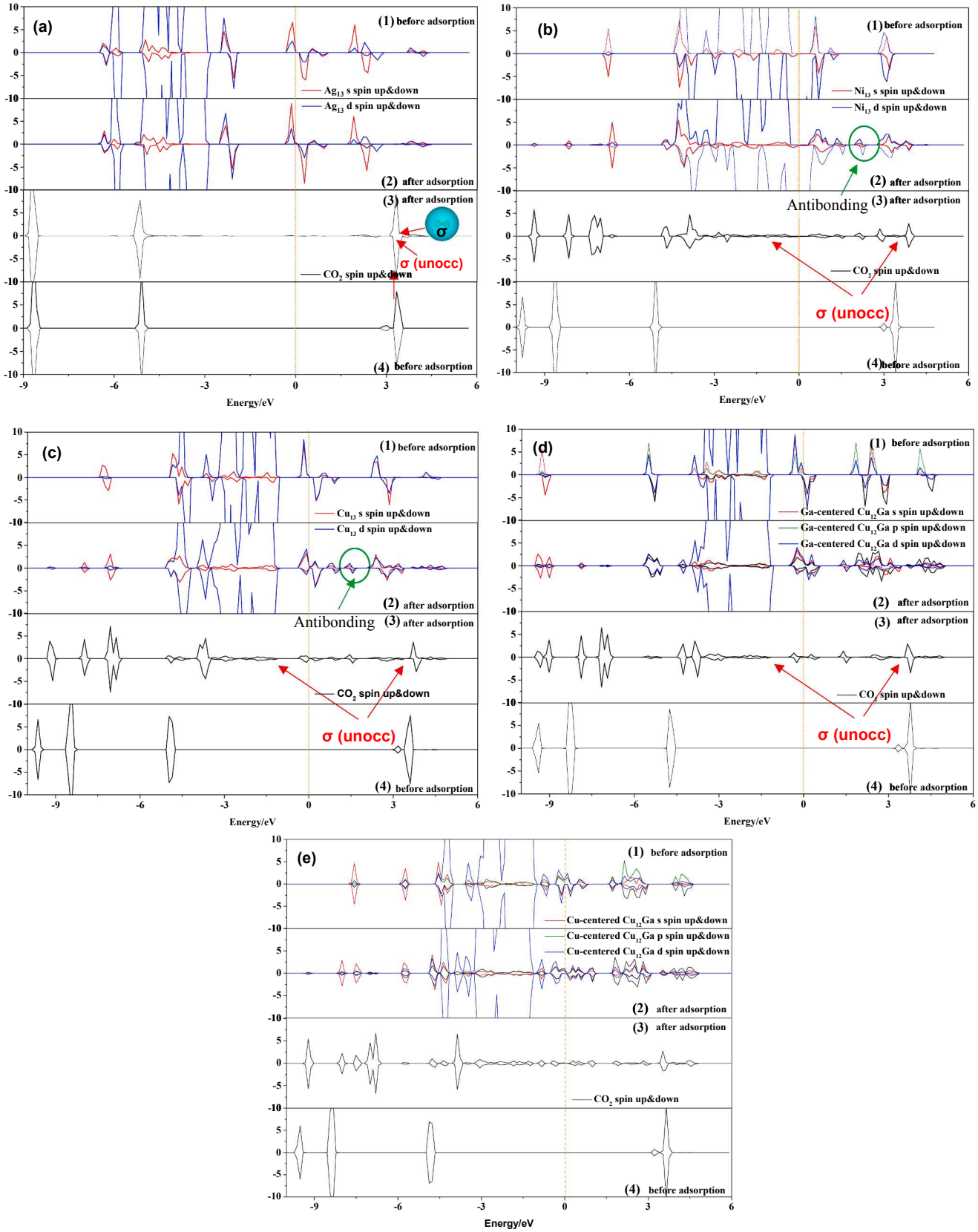

Fig. 5. (a) the PDOS of CO_2 and Ag_{13}, (b) the PDOS of CO_2 and Ni_{13}, (c) the PDOS of CO_2 and Cu_{13}, (d) the PDOS of CO_2 and Ga-centered $Cu_{12}Ga$, and (e) the PDOS of CO_2 and Cu-centered $Cu_{12}Ga$ before and after interaction.

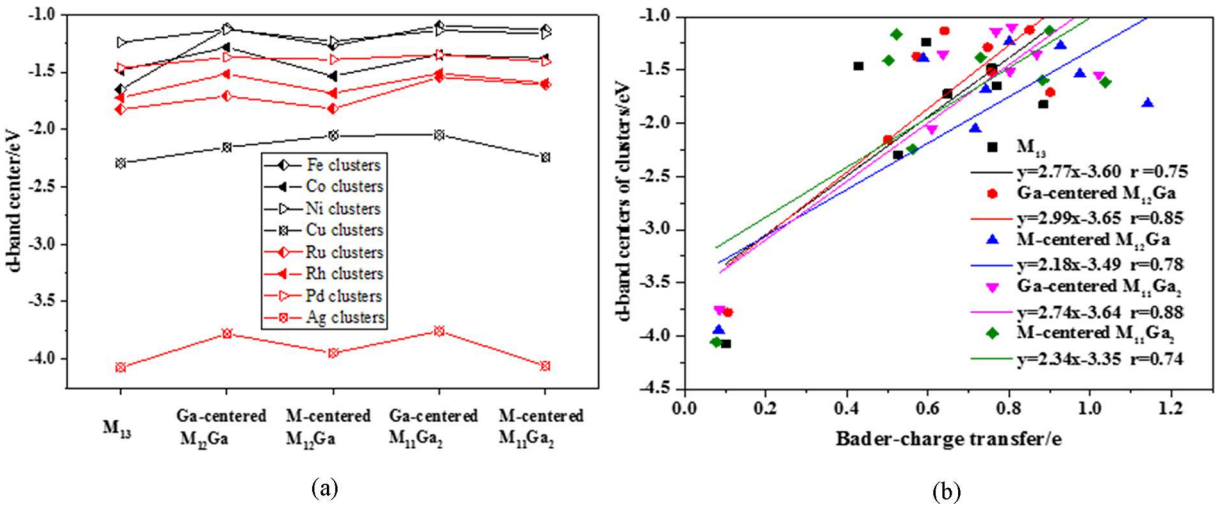

Fig. 6. (a) the d-band center of $M_{13-n}Ga_n$ clusters (b) the correlation between Bader charge transfers from clusters to CO_2 and d-band centers of $M_{13-n}Ga_n$ clusters.

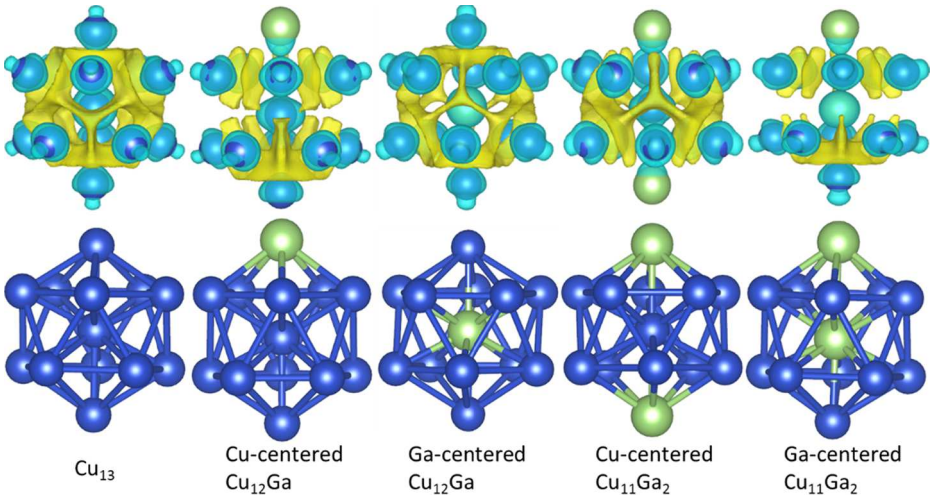

Fig. 7. Charge density differences of $Cu_{13-n}Ga_n$ clusters. Cyan and yellow represent the charge depletion and accumulation, respectively. (For interpretation of the references to colour in this figure legend, the reader is referred to the web version of this article.)

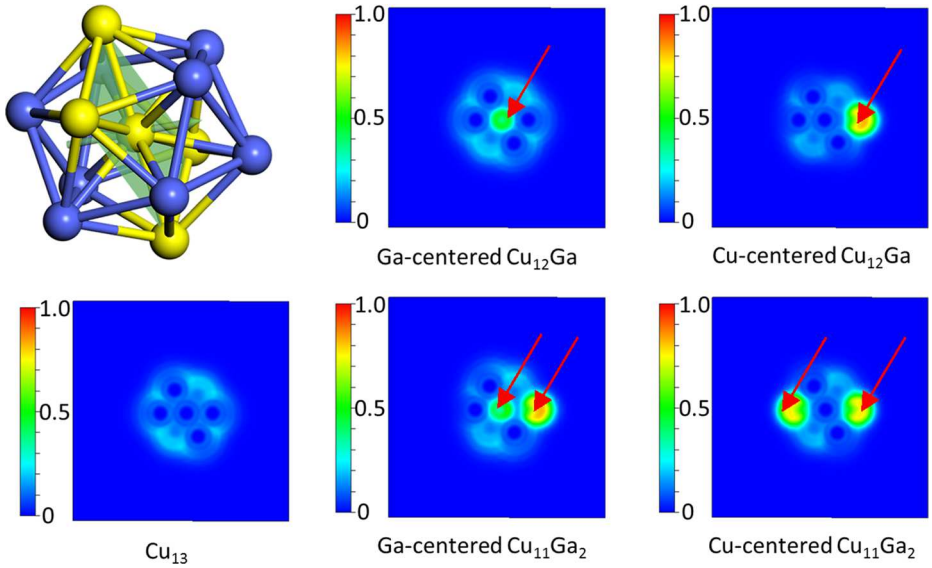

Fig. 8. The ELFs of $Cu_{13-n}Ga_n$ clusters.

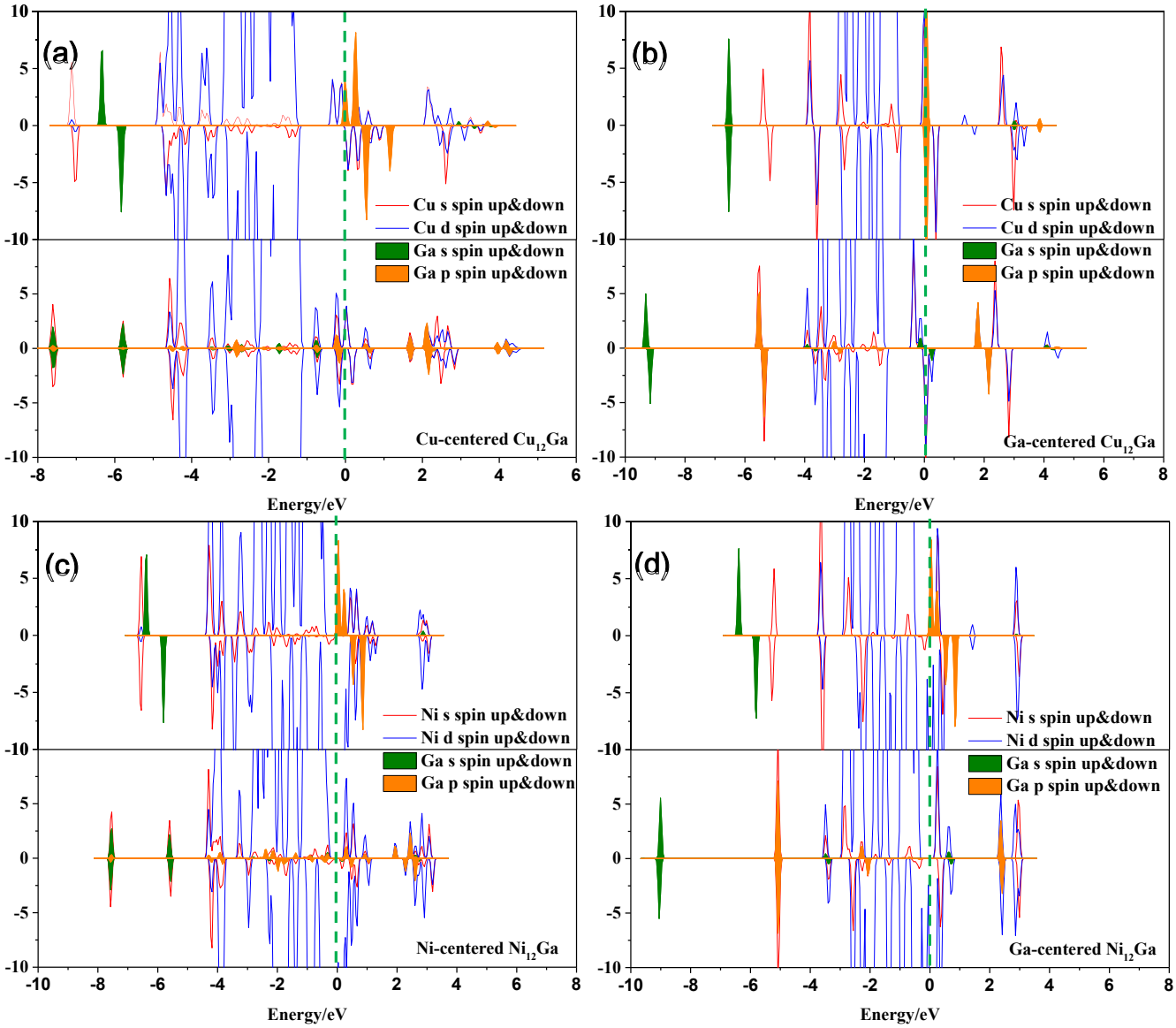

Fig. 9. The PDOS of Cu (Ni) and Ga in (a) Cu-centered $Cu_{12}Ga$, (b) Ga-centered $Cu_{12}Ga$, (c) Ni-centered $Ni_{12}Ga$, and (d) Ga-centered $Ni_{12}Ga$.

atom, and around it, there are free electrons. While for center Ga, the degree of localization is lower than that of Ga at the surface site. In addition, the concentration of free electron gas around Ga is greater than that of Cu. The results can well explain that the values of Bader charge transfer from Ga to Cu for Cu-centered $Cu_{13-n}Ga_n$ clusters are lower than for their corresponding Ga-centered clusters. However, one question arises: why center Ga transfers more electron density to Cu than surface Ga, but the structures with surface Ga transfer more electron density to CO_2. To answer this question, the following part is conducted. Fig. 3. The correlation between (a) Bader charge transfers from clusters to CO_2 and angles of adsorbed CO_2, and (b) Bader charge transfers from clusters to CO_2 and average C-O bond lengths of adsorbed CO_2.

3.3.3. The orbitals interactions of Ga and M atom in Ga doped $M_{13-n}Ga_n$ clusters and the influence on CO_2 adsorption

To answer the arising question and further probe into the structure effects of clusters on CO_2 adsorption, the PDOS of $M_{12}Ga$ clusters are analyzed. The PDOS of $Cu_{12}Ga$ and $Ni_{12}Ga$ clusters are displayed in Fig. 9(a)–(d), those of other clusters are displayed in Fig. S4 of Supplementary Materials. The top of the figure shows the PDOS of M_{12} and free Ga atom, the bottom illustrates the DOS projected on s and d orbitals of M and on s and p orbitals of Ga in $M_{12}Ga$ clusters. The difference in electronic configurations of Cu and Ni is the reason for choosing $Cu_{12}Ga$ and $Ni_{12}Ga$ as examples for analysis. It can be seen that, for Cu- (Ni-) centered $Cu_{12}Ga$ ($Ni_{12}Ga$) cluster, the s orbital of Ga mainly interact with the s orbital of Cu (Ni) far away from the Fermi level(0), the p orbitals of Ga mainly interacts with the d orbitals of Cu (Ni) near the Fermi level(0). Whereas for Ga-centered $Cu_{12}Ga$ ($Ni_{12}Ga$), the s and p orbitals of Ga interact only with the s orbital of Cu (Ni). In addition, from Fig. 9(a) and (b), one can clearly see that the value of occupied d orbital density of Cu increases, which means that there is electron transfer from Ga to Cu. The DOS analyses of CO_2 adsorption mentioned above shows that the adsorption of CO_2 on cluster is ascribed to the interaction of empty σ orbital of CO_2 with the s and d orbitals of cluster near the Fermi level(0). Therefore, in Ga-centered clusters, the interaction of Ga and M are almost ineffective to the adsorption of CO_2, while for M-centered clusters, the interaction of Ga affects this process.

4. Conclusions

Comprehensive DFT calculations were preformed to study activation of CO_2 by pure and Ga doped 3d and 4d 13-atom transition metal clusters ($M_{13-n}Ga_n$). We concluded that Ga doped Cu, Pd and Ag clusters are more stable than their analogues pure metal clusters. M-centered clusters are more stable than their corresponding Ga-centered clusters except Ga doped Pd and Ag clusters. For all the clusters, CO_2 favors to adsorb at the M composed bridge or hollow sites on $M_{13-n}Ga_n$ clusters except on $Ag_{13-n}Ga_n$ clusters. Most of Ga doped clusters can transfer more Bader charge density to CO_2 than pure clusters, but Ga doped Ag clusters do not change much compared with Ag_{13} clusters. In addition, the activation of CO_2 is well reflected by its structure deformation rather than with its adsorption energy.

The electronic properties of clusters greatly affect their catalytic properties. The replacement of M by Ga in M_{13} clusters has shifted up the d-band centers of clusters, and thus has improved their interactions with CO_2. Ga transfers electrons to M atoms in $M_{13-n}Ga_n$ clusters and centered Ga atom can transfer more electrons than surface located Ga. However, the numbers of effective electron transfer to CO_2 are similar for both Ga- and M-centered clusters. The empty σ orbital of CO_2 is the electron acceptor. The larger energy drop of σ orbital of CO_2 occurs, the more active CO_2 is. In addition, the nature of CO_2 adsorption on clusters relates to the interaction of σ orbital of CO_2 with the d orbitals of cluster near the Fermi level. The effective interaction of Ga and M relates to the p orbitals of Ga with d orbitals of M, which explains that M-centered $M_{12}Ga$ clusters can make CO_2 more active. This finding helps to design and produce efficient CO_2 activation materials and sheds a light on the details of their molecular and electronic structures.

CRediT authorship contribution statement

Qingli Tang: Conceptualization, Data curation, Formal analysis, Funding acquisition, Project administration, Visualization, Writing - original draft, Writing - review & editing. **Feng Shi:** Investigation, Methodology, Visualization, Writing - review & editing. **Kan Li:** Investigation, Methodology, Visualization, Writing - review & editing. **Wenchao Ji:** Formal analysis, Software. **Jerzy Leszczynski:** Software, Validation, Writing - original draft, Writing - review & editing. **Armistead G. Russell:** Software, Validation, Writing - original draft. **Eric G. Eddings:** Software, Validation, Writing - original draft. **Zhemin Shen:** Conceptualization, Data curation, Formal analysis, Funding acquisition, Project administration, Resources, Supervision, Writing - original draft, Writing - review & editing. **Maohong Fan:** Conceptualization, Formal analysis, Funding acquisition, Resources, Software, Supervision, Writing - original draft, Writing - review & editing.

Declaration of Competing Interest

The authors declare that they have no known competing financial interests or personal relationships that could have appeared to influence the work reported in this paper.

Acknowledgements

This work was funded by China Postdoctoral Science Foundation (2018M641999). Also, the authors also thank the USNSF-sponsored NCAR-Wyoming Supercomputing Center (NWSC), and National Science Foundation (NSF 1632899 and 1430001).

Appendix A. Supplementary data

Supplementary data to this article can be found online at https://doi.org/10.1016/j.fuel.2020.118446.

References

[1] Lu Y, Chen W. Sub-nanometre sized metal clusters: from synthetic challenges to the unique property discoveries. Chem Soc Rev 2012;41:3594–623.
[2] Lei Y, Mehmood F, Lee S, Greeley J, Lee B, Seifert S, et al. Increased silver activity for direct propylene epoxidation via subnanometer size effects. Science 2010;328:224–8.
[3] Turner M, Golovko VB, Vaughan OP, Abdulkin P, Berenguer-Murcia A, Tikhov MS, et al. Selective oxidation with dioxygen by gold nanoparticle catalysts derived from 55-atom clusters. Nature 2008;454:981–3.
[4] Vajda S, Pellin MJ, Greeley JP, Marshall CL, Curtiss LA, Ballentine GA, et al. Subnanometre platinum clusters as highly active and selective catalysts for the oxidative dehydrogenation of propane. Nat Mater 2009;8:213–6.
[5] Ishida T, Honma T, Nakada K, Murayama H, Mamba T, Kume K, et al. Pd-catalyzed decarbonylation of furfural: elucidation of support effect on Pd size and catalytic activity using in-situ XAFS. J Catal 2019;374:320–7.
[6] Qiao B, Wang A, Yang X, Allard LF, Jiang Z, Cui Y, et al. Single-atom catalysis of CO oxidation using Pt_1/FeO_x. Nat Chem 2011;3:634–41.
[7] Zhang H, Cui C, Luo Z. The doping effect of 13-Atom iron clusters on water adsorption and O-H bond dissociation. J Phys Chem A 2019;123:4891–9.
[8] Ocampo-Restrepo VK, Zibordi-Besse L, Da Silva JLF. Ab initio investigation of the atomistic descriptors in the activation of small molecules on 3d transition-metal 13-atom clusters: the example of H_2, CO, H_2O, and CO_2. J Chem Phys 2019;151:214301.
[9] Zhao F, Liu C, Wang P, Huang S, Tian H. First-principles investigations of the structural, electronic, and magnetic properties of $Pt_{13-n}Ni_n$ clusters. J Alloys Compd 2013;577:669–76.
[10] Zhang R, Peng M, Duan T, Wang B. Insight into size dependence of C_2 oxygenate synthesis from syngas on Cu cluster: the effect of cluster size on the selectivity. Appl Surf Sci 2017;407:282–96.
[11] Zhao B, Zhang R, Huang Z, Wang B. Effect of the size of Cu clusters on selectivity and activity of acetylene selective hydrogenation. Appl Catal A-Gen 2017;546:111–21.
[12] Ling L, Fan L, Feng X, Wang B, Zhang R. Effects of the size and Cu modulation of Pd_n ($n \leq 38$) clusters on Hg^0 adsorption. Chem Eng J 2017;308:289–98.
[13] Kim HY, Han SS, Ryu JH, Lee HM. Balance in adsorption energy of reactants steers CO oxidation mechanism of Ag_{13} and $Ag_{12}Pd_1$ nanoparticles: association mechanism versus carbonate-mediated mechanism. J Phys Chem C 2010;114:3156–60.
[14] de Graaf J, van Dillen AJ, de Jong KP, Koningsberger DC. Preparation of highly dispersed Pt particles in zeolite Y with a narrow particle size distribution: characterization by hydrogen chemisorption, TEM, EXAFS spectroscopy, and particle modeling. J Catal 2001;203:307–21.
[15] Liu X, Bauer M, Bertagnolli H, Roduner E, van Slageren J, Phillipp F. Structure and magnetization of small monodisperse platinum clusters. Phys Rev Lett 2006;97:253401.
[16] Bartolomé J, Bartolomé F, García LM, Roduner E, Akdogan Y, Wilhelm F, et al. Magnetization of Pt_{13} clusters supported in a NaY zeolite: a XANES and XMCD study. Phys Rev B 2009;80.
[17] Sun J, Cheng J. Solid-to-liquid phase transitions of sub-nanometer clusters enhance chemical transformation. Nat Commun 2019;10:5400.
[18] Shafai G, Hong S, Bertino M, Rahman TS. Effect of ligands on the geometric and electronic structure of Au_{13} clusters. J Phys Chem C 2009;113:12072–8.
[19] Koster AM, Calaminici P, Orgaz E, Roy DR, Reveles JU, Khanna SN. On the ground state of Pd_{13}. J Am Chem Soc 2011;133:12192–6.
[20] Watari N, Ohnishi S. Atomic and electronic structures of Pd_{13} and Pt_{13} clusters. Phys Rev B 1998;58:1665–77.
[21] Meng F, Gong Z, Wang Z, Fang P, Li X. Study on a nitrogen-doped porous carbon from oil sludge for CO_2 adsorption. Fuel 2019;251:562–71.
[22] Lai Q, Toan S, Assiri MA, Cheng H, Russell AG, Adidharma H, et al. Catalyst-TiO$(OH)_2$ could drastically reduce the energy consumption of CO_2 capture. Nat Commun 2018;9:2672.
[23] Ye R, Ding J, Gong W, Argyle M, Zhong Q, Wang Y, et al. CO_2 hydrogenation to high-value products via heterogeneous catalysis. Nat Commun 2019;10:15.
[24] Tang Q, Ji W, Russell CK, Cheng Z, Zhang Y, Fan M, et al. Understanding the catalytic mechanisms of CO_2 hydrogenation to methanol on unsupported and supported Ga-Ni clusters. Appl Energy 2019;253:113623.
[25] Tang Q, Ji W, Russell CK, Zhang Y, Fan M, Shen Z. A new and different insight into the promotion mechanisms of Ga for the hydrogenation of carbon dioxide to methanol over a Ga-doped Ni(211) bimetallic catalyst. Nanoscale 2019;11:9969–79.
[26] Chen J, Wang X, Wu D, Zhang J, Ma Q, Gao X, et al. Hydrogenation of CO_2 to light olefins on CuZnZr@(Zn-)SAPO-34 catalysts: Strategy for product distribution. Fuel 2019;239:44–52.
[27] Xiong S, Lian Y, Xie H, Liu B. Hydrogenation of CO_2 to methanol over Cu/ZnCr catalyst. Fuel 2019;256:5.
[28] Rui N, Wang Z, Sun K, Ye J, Ge Q. Liu C-j. CO_2 hydrogenation to methanol over Pd/In_2O_3: Effects of Pd and oxygen vacancy. Appl Catal B-Environ 2017;218:488–97.
[29] Chen P, Zhao G, Liu Y, Lu Y. Monolithic $Ni_5Ga_3/SiO_2/Al_2O_3$/Al-fiber catalyst for CO_2 hydrogenation to methanol at ambient pressure. Appl Catal A-Gen 2018;562:234–40.
[30] Frei MS, Capdevila-Cortada M, Garcia-Muelas R, Mondelli C, Lopez N, Stewart JA, et al. Mechanism and microkinetics of methanol synthesis via CO2 hydrogenation on indium oxide. J Catal 2018;361:313–21.
[31] Zhang X, Liu J-X, Zijlstra B, Filot IAW, Zhou Z, Sun S, et al. Optimum Cu nanoparticle catalysts for CO2 hydrogenation towards methanol. Nano Energy

2018;43:200–9.
[32] Porosoff MD, Yan B, Chen JG. Catalytic reduction of CO_2 by H_2 for synthesis of CO, methanol and hydrocarbons: challenges and opportunities. Energy Environ Sci 2016;9:62–73.
[33] Chen J, Luo Z. Single-point attack of two H_2O molecules towards a Lewis acid site on the $GaAl_{12}$ clusters for hydrogen evolution. ChemPhysChem 2019;20:499–505.
[34] Studt F, Sharafutdinov I, Abild-Pedersen F, Elkjaer CF, Hummelshoj JS, Dahl S, et al. Discovery of a Ni-Ga catalyst for carbon dioxide reduction to methanol. Nat Chem 2014;6:320–4.
[35] Fiordaliso EM, Sharafutdinov I, Carvalho HWP, Grunwaldt JD, Hansen TW, Chorkendorff I, et al. Intermetallic $GaPd_2$ nanoparticles on SiO_2 for low-pressure CO_2 hydrogenation to methanol: catalytic performance and in situ characterization. ACS Catal 2015;5:5827–36.
[36] Ladera R, Pérez-Alonso FJ, González-Carballo JM, Ojeda M, Rojas S, Fierro JLG. Catalytic valorization of CO_2 via methanol synthesis with Ga-promoted Cu-ZnO-ZrO_2 catalysts. Appl Catal B-Environ 2013;142–143:241–8.
[37] Toyir J, de la Piscina PR, Fierro JLG, Homs N. Catalytic performance for CO_2 conversion to methanol of gallium-promoted copper-based catalysts: Influence of metallic precursors. Appl Catal B-Environ 2001;34:255–66.
[38] Collins SE, Baltanas MA, Bonivardi AL. An infrared study of the intermediates of methanol synthesis from carbon dioxide over Pd/β-Ga_2O_3. J Catal 2004;226:410–21.
[39] Collins SE, Delgado JJ, Mira C, Calvino JJ, Bernal S, Chiavassa DL, et al. The role of Pd-Ga bimetallic particles in the bifunctional mechanism of selective methanol synthesis via CO_2 hydrogenation on a Pd/Ga_2O_3 catalyst. J Catal 2012;292:90–8.
[40] Medina JC, Figueroa M, Manrique R, Pereira JR, Srinivasan PD, Bravo-Saurez JJ, et al. Catalytic consequences of Ga promotion on Cu for CO_2 hydrogenation to methanol. Catal Sci Technol 2017;7:3375–87.
[41] Santiago-Rodriguez Y, Barreto-Rodriguez E, Curet-Arana MC. Quantum mechanical study of CO_2 and CO hydrogenation on Cu(111) surfaces doped with Ga, Mg, and Ti. J Mol Catal A-Chem 2016;423:319–32.
[42] Li SF, Guo ZX. CO_2 activation and total reduction on titanium(0001) surface. J Phys Chem C 2010;114:11456–9.
[43] Kresse G, Hafner J. Ab initio molecular dynamics for liquid metals. Phys Rev B 1993;47:558–61.
[44] Kresse G, Furthmuller J. Efficient iterative schemes for ab initio total-energy calculations using a plane-wave basis set. Phys Rev B 1996;54:11169–86.
[45] Kresse G, Furthmiiller J. Efficiency of ab-initio total energy calculations for metals and semiconductors using a plane-wave basis set. Comp Mater Sci 1996;6:15–50.
[46] Perdew JP, Burke K, Ernzerhof M. Generalized gradient approximation made simple. Phys Rev Lett 1996;77:3865–8.
[47] Blöchl PE. Projector augmented-wave method. Phys Rev B 1994;50:17953–79.
[48] Kresse G, Joubert D. From ultrasoft pseudopotentials to the projector augmented-wave method. Phys Rev B 1999;59:1758–75.
[49] Liu C, Cundari TR, Wilson AK. CO2 reduction on transition metal (Fe Co, Ni, and Cu) surfaces: In comparison with homogeneous catalysis. J Phys Chem C 2012;116:5681–8.
[50] Henkelman G, Arnaldsson A, Jónsson H. A fast and robust algorithm for Bader decomposition of charge density. Comp Mater Sci 2006;36:354–60.
[51] Sanville E, Kenny SD, Smith R, Henkelman G. Improved grid-based algorithm for Bader charge allocation. J Comput Chem 2007;28:899–908.
[52] Tang W, Sanville E, Henkelman G. A grid-based Bader analysis algorithm without lattice bias. J Phys Condens Matter 2009;21:084204.
[53] Lin S, Huang J, Gao XM, Ye XX, Guo H. Theoretical insight into the reaction mechanism of ethanol steam reforming on Co(0001). J Phys Chem C 2015;119:2680–91.
[54] Hammer B, Norskov JK. Electronic factors determining the reactivity of metal surfaces. Surf Sci 1995;343:211–20.
[55] Hammer BN, J K. Why gold is the noblest of all the metals. Nature 1995;376:238-40.
[56] Tian X, Zhao X, Su Y-Q, Wang L, Wang H, Dang D, et al. Engineering bunched Pt-Ni alloy nanocages for efficient oxygen reduction in practical fuel cells. Science 2019;366:850.
[57] Zhang H, Li Y, Hou J, Tu K, Chen Z. FeB_6 monolayers: The graphene-like material with hypercoordinate transition metal. J Am Chem Soc 2016;138:5644–51.
[58] Lu T, Chen Q. Revealing molecular electronic structure via analysis of valence electron density. Acta Phys-Chim Sin 2018;34:503–13.